2021

CFD Analysis of A Twin Screw Compressor with Oil Injection

Junfeng Wang
Simerics Inc, jw@simerics.com

Hui Ding
Simerics Inc

Sham Rane

Ahmed Kovacevic
University of London

CFD Analysis of a Twin Screw Compressor with Oil Injection

Junfeng WANG[1*], Hui DING[1], Sham RANE[2], Ahmed KOVACEVIC[2]

[1] Simerics Inc.,
1750 112th AVE NE Ste C205, Bellevue, WA 98004, USA
jw@simerics.com

[2] Centre for Compressor Technology, City, University of London,
London, UK
sham.rane@city.ac.uk, A.Kovacevic@city.ac.uk

* Corresponding Author

ABSTRACT

In this paper, a full 3D transient Computational Fluid Dynamics (CFD) model of a twin screw compressor with oil injection is described in detail. Volume of Fluid (VOF) two phase flow model is used for gas and liquid phases. The rotor meshes are generated by *SCORG*^{TM} grid generator and read into the CFD solver at each time step. The simulation runs efficiently and results are obtained in about 12 hours on 24 CPU cores. The CFD prediction of air mass flow rate and indicated power has a good agreement with the experimental data measured at City University of London. The compression pocket is tracked using a customized post-processing technique and the pressure-volume diagram within it is also obtained and analyzed. Simulations demonstrate that the approaches used in this paper are robust and fast, and can be readily applied to industrial compressor systems for rapid design iterations and improvements.

1. INTRODUCTION

A rotary twin screw compressor is commonly used in a wide variety of industrial applications due to its reliability, compact structure and wide range of operating pressures and flow rates. Comparing to the dry twin screw compressor, the added oil in oil flooded twin screw compressor offers several advantages. Most importantly, the oil can significantly reduce the gas temperature in the compression chamber as well as the rotor temperature to prevent seizure. Secondly, the oil can seal clearance gaps to improve volumetric efficiency. Thirdly, the oil lubricates rotors and bearings. It is also essential to optimize the oil injection to reduce the power loss associated with the oil for a better performance. However, it is extremely difficult to experimentally determine oil distribution.

Recently, 3D CFD simulation gradually gains its popularity because CFD simulations can deliver deep insights into the performance of a twin screw compressor and provide detailed flow pattern of oil and gas. However, 3D CFD transient simulations faced several challenges. In earlier days, the major challenge was the complex deforming fluid domain in the screw compressor chamber, which required a robust CFD grid to deal with. This difficulty prevented the broad application of CFD simulations to twin screw compressors. A breakthrough was achieved by Kovacevic (Kovacevic, 2002, 2005) who applied the analytical rack generation method of Stosic (Stosic, 1998) to generate an algebraic, adaptive block-structured grid. Screw Compressor Rotor Grid Generator (SCORG) was then developed to generate grids and pre-processing scripts for other CFD software to use. Rane (S. Rane, 2015) proposed a new approach to generate a conformal interface between the rotor domains to improve the accuracy of indicated power and flow rate. The rotor meshes generated by the conformal way are employed in this study. Another challenge is to solve two phase flow with complex moving parts and small leakage gaps. The high density ratio between liquid and gas, sophisticated interaction among the phases, and the interface tracking with complex shape makes the problem difficult to solve. In such case, gas phase has to be treated as compressible, heat transfer effects have to be included, and interface tracking has to be done inside moving, deforming volumes. The major issues for such multiphase CFD simulations are poor convergence, very long simulation time, and unsatisfactory mass/energy conservation. Ding (Ding & Jiang, 2017) performed a numerical simulation of an oil flooded twin screw compressor using CFD package Simerics-MP+ to show the cooling and sealing effects of oil. The simulation demonstrated good convergence, fast calculation speed, and excellent conservation of mass and energy. In this paper, a screw compressor with oil injection model is investigated

and validated with test data. The CFD model will be described in detail. Simulation results of indicated power and gas flow rate will be compared with the experimental data. Oil distribution and temperature distribution will be visualized and analyzed.

2. CFD SOLVER AND GOVERNING EQUATIONS

2.1 Conservation Equations for Gas Liquid Mixture

The CFD package Simerics-MP+ is employed to perform the numerical simulations. In Simerics-MP+, the conservation of mass, momentum, and energy of a compressible fluid are solved using finite volume method. These conservation laws can be written in integral representation as

$$\frac{\partial}{\partial t}\int_{\Omega(t)}\rho d\Omega + \int_{\sigma}\rho(\mathbf{v}-\mathbf{v_\sigma})\cdot\mathbf{n}d\sigma = 0 \tag{1}$$

$$\frac{\partial}{\partial t}\int_{\Omega(t)}\rho\mathbf{v}d\Omega + \int_{\sigma}\rho((\mathbf{v}-\mathbf{v_\sigma})\cdot\mathbf{n})\mathbf{v}d\sigma = \int_{\sigma}\boldsymbol{\tau}\cdot\mathbf{n}d\sigma - \int_{\sigma}p\mathbf{n}d\sigma + \int_{\Omega}\mathbf{f}d\Omega \tag{2}$$

$$\frac{\partial}{\partial t}\int_{\Omega(t)}\rho E d\Omega + \int_{\sigma}\rho((\mathbf{v}-\mathbf{v_\sigma})\cdot\mathbf{n})Ed\sigma = \int_{\sigma}\kappa\nabla T\cdot\mathbf{n}d\sigma - \int_{\sigma}p\mathbf{v}\cdot\mathbf{n}d\sigma + \int_{\sigma}(\mathbf{v}\cdot\boldsymbol{\tau})\cdot\mathbf{n}d\sigma + \int_{\Omega}\mathbf{f}\cdot\mathbf{v}d\Omega \tag{3}$$

in which $\Omega(t)$ is the volume of the computational domain or control volume, σ is the surface of $\Omega(t)$, $\mathbf{n}$ is the surface normal of σ pointed outwards, ρ is the fluid density, p is the pressure, $\mathbf{f}$ is the body force, $\mathbf{v}$ is the fluid velocity and $\mathbf{v_\sigma}$ is surface motion velocity. The shear stress tensor $\boldsymbol{\tau}$ is a function of the fluid viscosity μ and the velocity gradient.

The standard $k-\varepsilon$ two-equation model (Launder & Spalding, 1974) is used to account for turbulence,

$$\frac{\partial}{\partial t}\int_{\Omega(t)}\rho\kappa d\Omega + \int_{\sigma}\rho((\mathbf{v}-\mathbf{v_\sigma})\cdot\mathbf{n})\kappa d\sigma = \int_{\sigma}(\mu+\frac{\mu_t}{\sigma_\kappa})(\nabla\kappa\cdot\mathbf{n})d\sigma + \int_{\Omega}(G_t-\rho\varepsilon)d\Omega \tag{4}$$

$$\frac{\partial}{\partial t}\int_{\Omega(t)}\rho\varepsilon d\Omega + \int_{\sigma}\rho((\mathbf{v}-\mathbf{v_\sigma})\cdot\mathbf{n})\varepsilon d\sigma = \int_{\sigma}(\mu+\frac{\mu_t}{\sigma_\varepsilon})(\nabla\varepsilon\cdot\mathbf{n})d\sigma + \int_{\Omega}(c_1G_t\frac{\varepsilon}{\kappa}-c_2\rho\frac{\varepsilon^2}{\kappa})d\Omega \tag{5}$$

Together with equation of state, where density is a function of temperature and pressure, to form a closed system:

$$\rho = f(p,T) \tag{6}$$

2.2 VOF Model

VOF models are widely used in simulation of two phase flow (Hirt & Nichols, 1981)]. VOF solves a set of scalar transport equations representing the volume fraction of each fluid component occupies in every computational cell. The transport equation of the volume fraction for each fluid component can be written as:

$$\frac{\partial}{\partial t}\int_{\Omega(t)}\rho_i F_i d\Omega + \int_{\sigma}\rho_i(v-v_\sigma)\cdot\mathbf{n}F_i d\sigma = 0 \tag{7}$$

where F_i is the volume fraction of the ith fluid component, and ρ_i is the local density of ith fluid component. The weighted mixture density of the fluid in equation (1) to (5) are then calculated as:

$$\rho = \Sigma\rho_i F_i \tag{8}$$

Both implicit and explicit methods can be used to solve the equation. High Resolution Interface Capturing (HRIC) scheme can be used for the convective term in the transport equation.

3. CASE STUDY

The test compressor used for this study is an oil flooded twin screw compressor with a 4/5 lobe arrangement and 'N' profiles. The nominal interlobe, radial and axial leakage gaps are 60 μm. The main rotor diameter is 127.0 mm and the wrap angle is 306^o. The tests with different rotor speeds and discharge pressures were carried out at City University of London (A. Rane S.R. Kovacevic & Stosic, 2016) and the results have been used in this paper for comparison with those from Simerics-MP+.

3.1 CFD Model

Figure 1 and Figure 2 show the simulation fluid domain and the corresponding meshes in 3D view. The rotor part of the twin screw is meshed as a single domain using a grid generation software SCORG which creates a series of mesh files for the rotor at different rotation angles. The rotor mesh files are read into the solver via volume remesh approach. The suction port and discharge port of fluid volumes are meshed using Simerics-MP+ binary tree unstructured mesher. The oil injection is through four injection holes that are connected to the rotor domain. All the fluid volumes are connected together using Mis-matched Grid Interface (MGI). The total number of cells is about 0.795 million. Simulations under three operating conditions have been carried out, listed in Table 1.

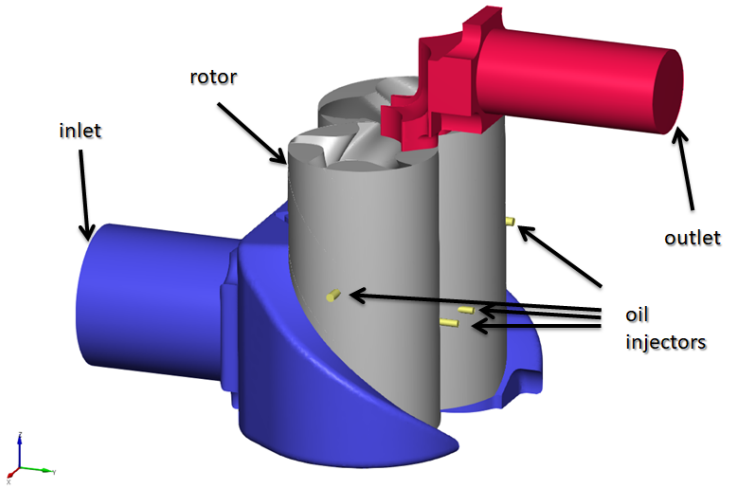

Figure 1: Fluid volume

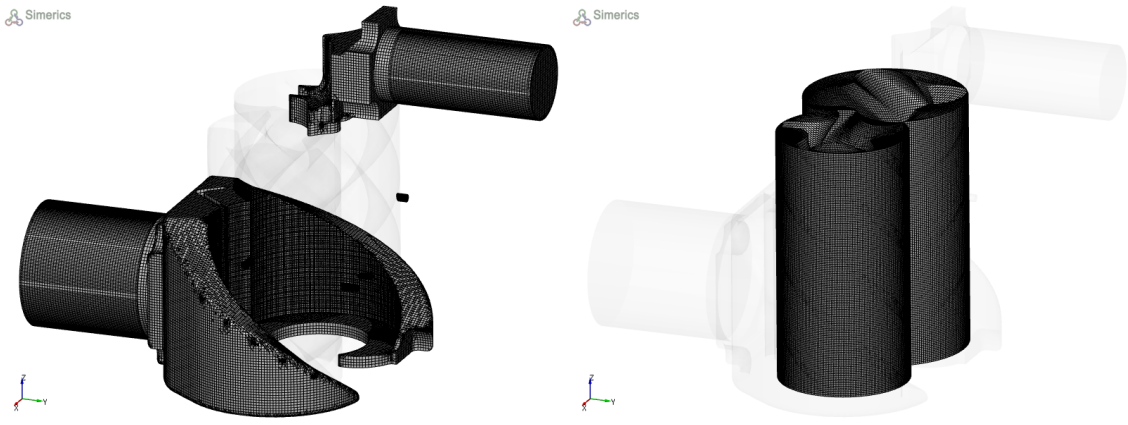

Figure 2: Ports and rotor meshes

The axial end clearances can be included in the CFD model without causing divergence or sacrificing running speed.

Table 1: CFD model cases and operating conditions

Case	Male Rotor Speed (rpm)	Suction Pressure (bar)	Suction Temperature (K)	Discharge Pressure (bar)	Oil Injection Pressure (bar)	Oil Injection Temperature (K)
1	3000	1.00	298.0	6.0	5.5	323.0
2	3000	1.00	298.0	8.0	7.5	323.0
3	6000	1.00	298.0	8.0	7.5	323.0

However, they are not included for simplification purpose. The air and oil properties are summarized in Table 2. The air phase is defined as an ideal gas state with molar mass of 28.96 kg/kmol.

Table 2: Gas and oil properties

	Gas	Oil
Density	Air (using ideal gas law)	800 kg/m^3
Specific heat capacity	1004.4 J/kgK	1800 J/kgK
Dynamic viscosity	1.831^{-5} $Pa \cdot s$	0.0088 $Pa \cdot s$
Thermal conductivity	0.0261 W/mK	0.18 W/mK

The discharge pressure is gradually increased to the designed pressure within 4 full male rotor rotations. Results becomes periodic within 15 revolutions for all simulations. Mass imbalance for air is below 3% and for oil phase is within 1.5%. The simulations are carried out at Dell PowerEdge computing nodes @ 2.2GHz. The simulation time is about 2.4 hours per revolution using 6 cores and is reduced to 0.84 hours per revolution on 24 cores.

3.2 Comparison of the Air Flow and Indicated Power with Experimental Results

Table 3 shows both predicted CFD results and experimental results of the air mass flow rate and the indicated power for three cases. It can be seen that for Case1 and Case2 at 3000 rpm the predicted air mass flow rates are below 3% of the experimental values. The air mass flow rate prediction in Case3 is 4% higher than the measured value. Comparing to the flow rate of Case2 at 3000 rpm, the flow rate of Case3 at 6000 rpm has increased by 87% which is slightly less than the ideal increasement factor of 1 due to the leakages and drop in suction air density. The indicated powers predicted by CFD simulations in Case1 and Case2 are 2% and 6% higher than the measured data respectively, while that in Case3 is above 7%. The indicated power in experiments is obtained by multiplying the measured shaft power with an estimated mechanical efficiency of 70%. This could underestimate the indicated power in experiments and is also the possible reason that CFD simulation predict higher powers than those in experiments.

Table 3: Comparison of the flow and indicated power with experimental results

	Air Mass Flow Rate (kg/min)			Indicated Power (kW)		
Case	Experimental result	CFD result	Difference	Experimental result	CFD result	Difference
1	4.73	4.58	-3%	16.31	16.65	2%
2	4.67	4.52	-3%	19.15	20.32	6%
3	8.75	9.10	4%	39.22	42.07	7%

3.3 Pressure-Volume Diagram

A user defined script is employed in the software to track the compression pocket as well as to calculate its volume and averaged pressure. Figure 3 shows the pressure contour of the compression pocket at different male rotor angles for Case2. The color map ranges from 1.0 bar to 8.0 bar. It can be seen that the pressure in the pocket is low when it is initially formed near the suction port and then the pressure increases with the pocket volume being reduced. The compression pocket averaged pressure and volume diagram is also shown in Figure 4. It is observed that for three cases the pressure during the compression process before connecting to the discharge port aligns closely. After the compression pocket connects to the discharge port, it is noted that Case3 with 6000 rpm and 8.0 bar discharge pressure

has the highest maximum pressure pulsation value of 10.5 bar, while Case1 with 3000 rpm and 6.0 bar discharge pressure has the lowest pressure pulsation.

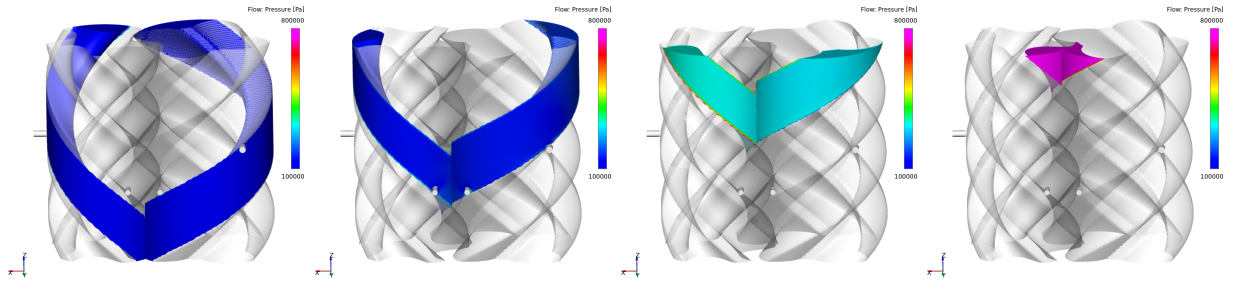

(a) **(b)** **(c)** **(d)**

Figure 3: Compression pocket and pocket pressure contour for Case2 at different male rotor angles: (a) 45^o (b) 135^o (c) 225^o (d) 315^o

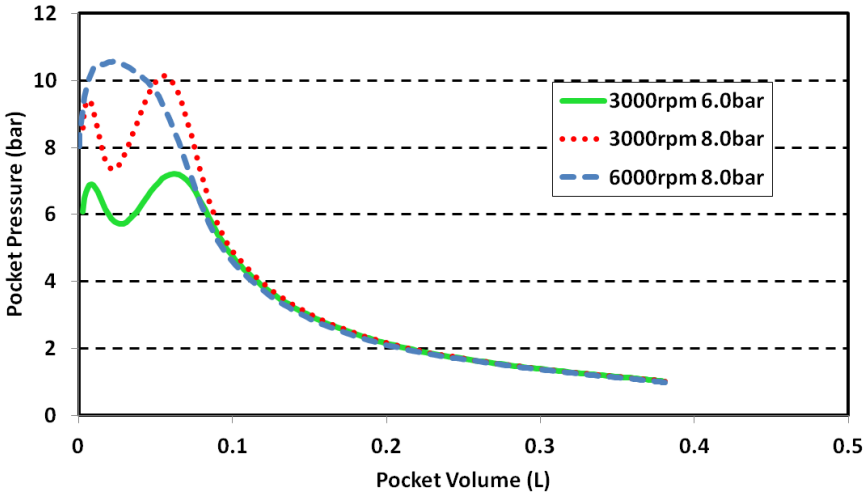

Figure 4: Averaged pressure and volume diagram of compression pocket

3.4 Oil Distribution

Figure 5 shows oil concentration contours at four different male rotor angles for Case2. The color map ranges from 0% to 15% volume fraction of oil with magenta representing high concentration and blue representing low concentration. Oil has higher concentration close to the injection and then been carried away by the movement of pocket. It is also observed that oil is accumulated in the rotor tips and discharge port. Figure 6 plots instantaneous oil flow rate at the discharge port for one complete male rotor cycle after solution becomes periodic. The oil flow rate for Case1 with 3000 rpm and 6.0 bar is lower than that of Case2 with same rotation speed but higher pressure 8.0 bar. Case3 with 6000 rpm and 8.0 bar exhibits bigger oscillation with higher maximum value and lower minimum value comparing to other Cases. This oil distribution variation has a direct impact on the temperature distribution, which will be discussed in detail in the next section.

3.5 Temperature Distribution

Figure 7 shows temperature contour for Case2 at four different male rotor angles. The color map ranges from 290 K to 350 K with magenta representing high temperature and blue representing low temperature. The temperature inside each pocket is highly non-uniform due to the cooling effects of injected oil. By comparing the temperature contour in Figure 7 with the oil distribution contour in Figure 5, it can been seen that typically higher oil concentration areas have lower temperature and lower oil concentration areas have higher temperature. As shown in Figure 8, the averaged temperature of mixture (both oil and air) at the discharge is periodic. Case3 with 6000 rpm and 8.0 bar has the maximum

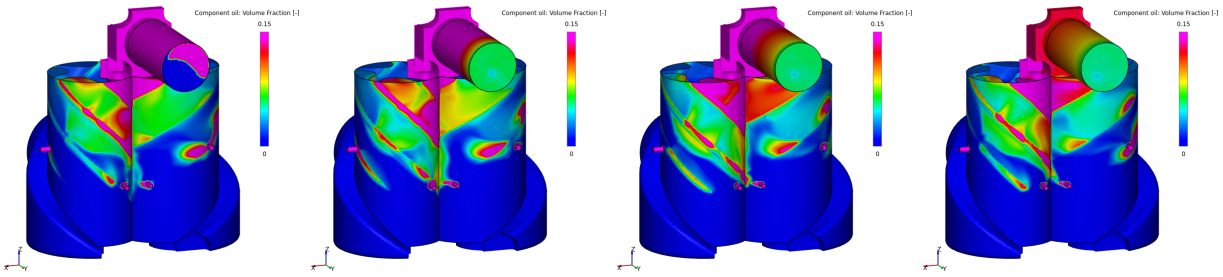

(a) **(b)** **(c)** **(d)**

Figure 5: Oil distribution for Case2 at different male rotor angles: (a) 45^o (b) 67.5^o (c) 90^o (d) 112.5^o

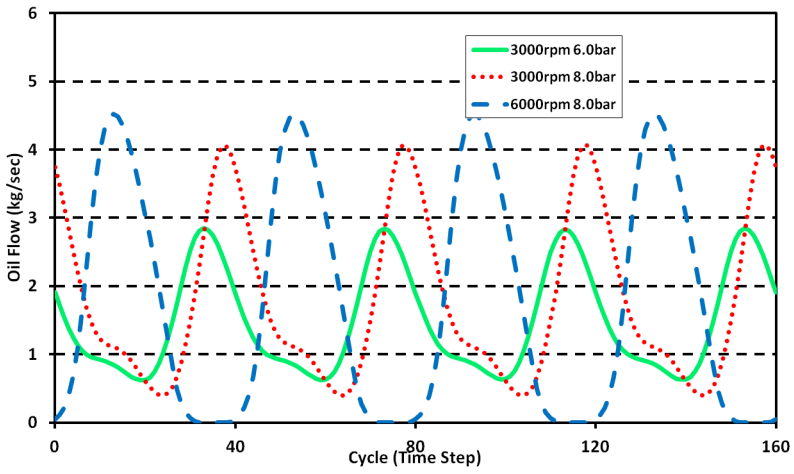

Figure 6: Oil mass flow at the discharge

peak temperature of 370 K around time steps at 0,40,80,120 and 160, which is resulted from the close to zero oil flow at the same time steps as shown in Figure 5. Other than these time steps, the temperature is lower since the oil flow is higher. Case 1 and Case2 exhibit the similar correlation between the oil distribution and temperature distribution, which has demonstrated the oil cooling effects.

There are three parameters that significantly impact the temperature in the compression chamber and discharge; a) Discharge Pressure, b) Rotational speed and c) Oil injection. With increase in both discharge pressure and rotational speed, the gas temperature increases due to higher compression work and lower residence time available for injected oil heat transfer. With increase in oil injection mass the gas temperature decreases. Both these effects have been observed from Figure 6,7 and 8.

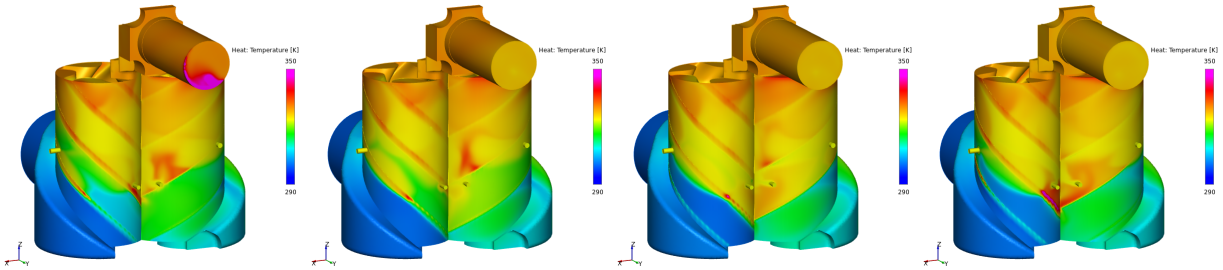

(a) **(b)** **(c)** **(d)**

Figure 7: Temperature distribution for Case2 at different male rotor angle: (a) 45^o (b) 67.5^o (c) 90^o (d) 112.5^o

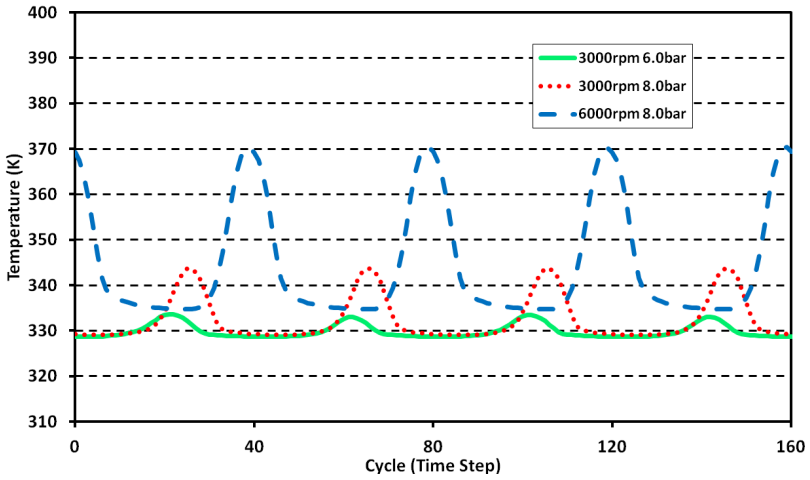

Figure 8: Averaged temperature at the discharge

4. CONCLUSIONS

This paper reports the CFD simulations for a twin screw compressor with oil injection using VOF multiphase model. The rotor mesh is generated by *SCORG*^{TM} and read into the solver at each time step. Three simulations at different rotor speeds and discharge pressures are performed. The results of gas flow rate and indicated power are compared with the experimental measurements in City, University of London.

- Gas mass flow rates in numerical simulations have a good agreement with the test values in three cases.
- The indicated powers obtained by numerical simulation show a well match with the measured shaft power.
- The averaged pressure in compression pocket is tracked and pressure-volume diagram is also plotted and compared for three cases.

- Oil distribution clearly exhibits the cooling effect on the temperature distribution.
- The solver provides a very efficient tool for numerical simulation and to better understand and improve the design.

NOMENCLATURE

Ω	control volume	(m^3)
σ	surface of control volume	(m^2)
$\mathbf{n}$	surface normal	(-)
ρ	fluid density	(kg/m^3)
p	pressure	(Pa)
$\mathbf{f}$	body force	(N)
$\mathbf{v}$	fluid velocity	(m/s)
$\mathbf{v_\sigma}$	surface motion velocity	(m/s)
$\boldsymbol{\tau}$	shear stress tensor	(-)
μ	fluid viscosity	$(Pa \cdot s)$
F	volume fraction	(-)

Subscript

i	fluid component

REFERENCES

Ding, H., & Jiang, Y. (2017). CFD simulation of a screw compressor with oil injection. *IOP Conference Series: Materials Science and Engineering*, *232*, 012020. Retrieved from https://doi.org/10.1088%2F1757-899x%2F232%2F1%2F012020 doi: 10.1088/1757-899x/232/1/012020

Hirt, C., & Nichols, B. (1981). Volume of fluid (vof) method for the dynamics of free boundaries. *Journal of Computational Physics*, *39*, 201-225.

Kovacevic, A. (2002). Three-dimensional numerical analysis for flow prediction in positive displacement screw machines. *Doctoral Thesis*.

Kovacevic, A. (2005). Boundary adaptation in grid generation for cfd analysis of screw compressors. *International Journal for Numerical Methods in Engineering*, *64*(3), 401-426.

Launder, B., & Spalding, D. (1974). The numerical computation of turbulent flows. *Computer Methods in Applied Mechanics and Engineering*, *3*, 269-289.

Rane, A., S.R. Kovacevic, & Stosic, N. (2016). Cfd analysis of oil flooded twin screw compressor. *International Compressor Engineering Conference*.

Rane, S. (2015). Grid generation and cfd analysis of variable geometry screw machines. *Doctoral Thesis*.

Stosic, N. (1998). On gearing of helical screw compressor rotors. *Proceedings of the Institution of Mechanical Engineers, Part C: Journal of Mechanical Engineering Science*, *212*, 587-594.